MODELING ROTOR DYNAMICS WITH ROTOR SPEED DEGREE OF FREEDOM FOR DRIVE TRAIN TORSIONAL STABILITY ANALYSIS

Link C. Jaw [i]
Garrett Engine Div. of Allied-Signal Aerospace Company
Phoenix, Arizona, U. S. A.

Arthur E. Bryson, Jr. [ii]
Stanford University, Stanford, California, U. S. A.

September 21, 1990

1 Abstract

Incompatibilities in the rotor/engine system torsional dynamics may cause torque oscillation and rotor speed variations, and they affect the handling qualities of a vehicle.

To analyze torsional stability, the coupling between rotor and engine systems must be considered. This coupling is represented by the rotor speed DOF. The effect of this DOF is to increase the natural frequency and damping ratio of the collective lead-lag mode.

Torsional resonances can be predicted by a simplified mass-spring-damper model. The generic spring-damper model was found inadequate; consequently, two improvements for this model are proposed in this paper.

2 Nomenclature

B	Blade Tip Loss Factor
b	Linear Damping Coefficient
c	Blade Chord Length
c_{d_0}	Profile Drag Coefficient
e	Blade Hinge Offset
I	Blade Moment of Inertia
$\mathbf{I}$	Identity Matrix
J	Shaft Moment of Inertia
k	Spring Constant
m	Mass
Q	Torque
r_R	Blade Root Cut-Out Factor
s	Laplace Variable
y_g	Blade Spanwise Distance between Hinge and C. M.

Greek Symbols

β	Flap Angle
ξ	Lead-Lag Angle
ρ	Air Density
ψ	Rotor Hub Angle or Blade Angle
Ω	Rotor Angular Speed
ω	Angular Speed

Subsripts

b	Rotor Blade
e	Engine
f	Fuselage
h	Main Rotor Hub
l	Load Distrubance or Lag Spring
lh	Lag Hinge
mb	Multi-Blade
mr	Main Rotor
nr	Non-Rotating Coordinate System
q	Torque
t	Tansmission Shaft Spring
tr	Tail Rotor
0	Blade Collective Coefficient
$1c$	Longitudinal Cyclic Coefficient
$1s$	Lateral Cyclic Coefficient

3 Introduction

A helicopter and its propulsion system represent two different engineering disciplines, and they are usually designed and manufactured by different companies. When the two systems are put together, incompatibilities often occur, which could affect flight safety and performance. In particular, the rotor/engine system torsional dynamics may cause torque oscillations and rotor speed variations, and they affect the handling qualities of the vehicle.

Frederickson, Rumford, and Stephenson [5] reported a fuel control stability problem on CH-47C helicopter, where a 4.1 *Hz* torque oscillation with a magnitude of 8-12% of the maximum steady torque was observed. The problem was corrected by softening the blade lag damper springs and reducing fuel control gain by 30%. The most complete investigation

[i] Engineering Specialist.
[ii] Pigott Professor of Engineering, Department of Aeronautics and Astronautics.

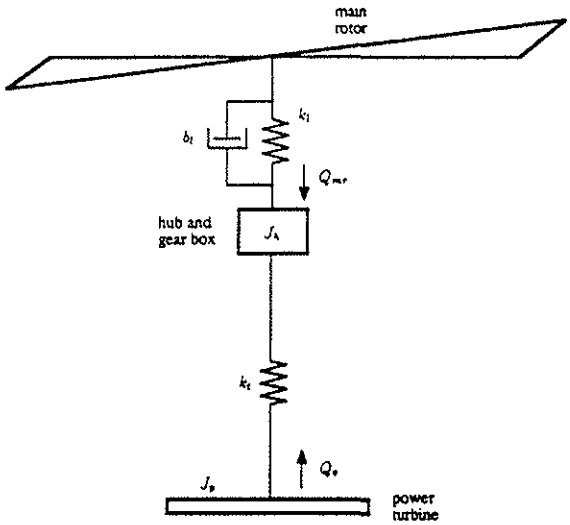

Figure 1: Suggested Linear Model for Rotor-Engine Torsional Compatibility Studies

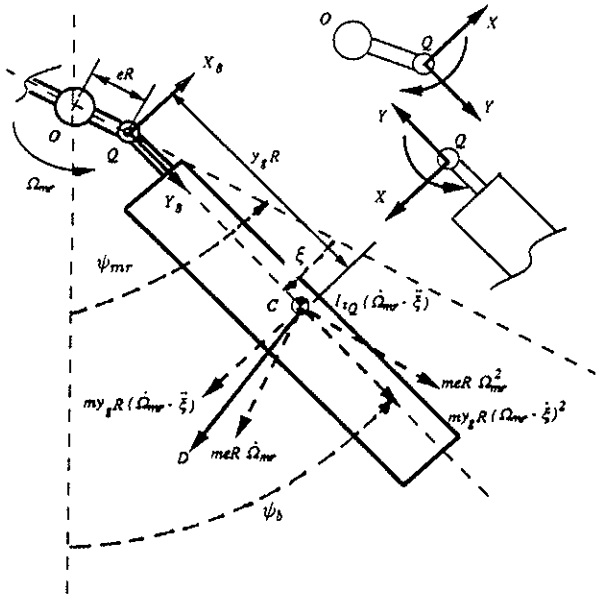

Figure 2: A Hypothetical Single-Bladed Rotor

of airframe/engine compatibility problems was documented by major U. S. helicopter manufacturers in a series of U. S. Army sponsored programs in late 70's (cf. [12], [11], [15], [2], and [6]). The problems related to torsional stability are characterized by unacceptable shaft torque and speed oscillations, mostly on articulated-rotor helicopters.

To analyze torsional stability, the Society of Automotive Engineers [13] has suggested a simple, linear model shown in Figure 1, where k_l is the *effective* lead-lag spring constant, and b_l is the *effective* damper coefficient. The spring constant comes from the centrifugal force of blades. This simplified model allows torsional flexible modes to be predicted by engine manufacturers in their designs of fuel control. However, the accuracy of this analysis depends on good estimates of what the spring constant and damper coefficient are.

Typically, the spring constant from the centrifugal force acting on the blades and the lag damper coefficient are used; however, from experience, the resonant frequency is often over-predicted. This suggests that some other factors be considered in modeling the resonance phenomenon.

This paper analyzes the dynamics of an articulated rotor system in hover with a shaft/rotor speed DOF. The rotor speed DOF comes from the coupling between the rotor and the engine. It is shown that this coupling increases the natural frequency and damping ratio of the collective lead-lag mode.

From the analyses of simplified rotor models, two improvements for the generic model are proposed.

Analytical results are substantiated by the simulated rotor system of the Black Hawk helicopter.

4 Lead-Lag Dynamics of a Hypothetical One-Bladed Rotor

Consider a hypothetical rotor with only one hinged, rectangular blade having in-plane, lead-lag motion. For simplicity, we assume that it is on a *hovering* helicopter (the mechanical imbalance problem is not considered here). Figure 2 shows the blade moving backward (opposite to the shaft rotation) to form a lag angle, ξ , between the blade span axis, y_B , and the reference line of the blade azimuth angle.

Also shown in Figure 2 are the drag (D) and various d'Alembert forces acting through the blade center of mass, C. The blade is assumed to produce zero lift; therefore, no flapping motion exists. The properties of this hypothetical blade are listed in Table 1.

4.1 Equations of Motion

The equation of motion for the blade, assuming that hub angular speed, Ω_{mr}, is held constant, is given by

$$I_{z_Q}\,\ddot{\xi} + b_{lh}\,\dot{\xi} + mey_g R^2\Omega_{mr}^2\,\xi \approx y_g RD \qquad (1)$$

where $I_{z_Q} = I_{z_C} + my_g^2 R^2$ is the blade moment of inertia about the hinge, b_{lh} is the lag damper coefficient, and the stiffness comes from the centrifugal force acting through the blade's center of mass (commonly called the centrifugal spring).

When rotor speed varies, the coupling between the blade and its hub changes the characteristics of the lead-lag dynamics above. The equations of motion for this simplified rotor are derived in Appendix A. From

Variables	Values
R	$25\,ft$
c	$2\,ft$
Ω_{mr}	$27\,rad/sec$
r_R	0.1
B	0.95
e	0.05
y_g	0.5
c_{d_0}	0.05
m	$7.4\,slug$
I_{z_Q}	$1400\,slug-ft^2$
J_h	$1100\,slug-ft^2$
b_{lh}	$2200\,lb-sec$

Table 1: Properties of a Hypothetical Blade

Equations (101) and (97),

$$\begin{aligned}\ddot{\xi} &= -\left(\frac{k_c}{I_{z_Q}}+c_1d_1eRq_1\Omega_{mr_0}^2\right)\delta\xi \\ &\quad -\left(\frac{b'_{lh}}{I_{z_Q}}+c_1d_1eRq_2''\right)\dot{\xi} \\ &\quad -c_1d_1h_\omega\,\delta\Omega_{mr}+c_1d_1\,\delta Q_{e_r}\,, \qquad (2)\\ \dot{\Omega}_{mr} &= -d_1eRq_1\Omega_{mr_0}^2\,\delta\xi \\ &\quad -d_1eRq_2''\,\dot{\xi}-d_1h_\omega\,\delta\Omega_{mr}+d_1\,\delta Q_{e_r}\,; \qquad (3)\end{aligned}$$

where,

$$k_c \equiv mey_gR^2\Omega_{mr_0}^2\,. \qquad (4)$$

Note that the natural frequency and damping of blade lead-lag oscillation have both been *increased* from their respective constant-rotor speed values (in Equation (1)) due to *blade-hub coupling*.

4.2 Describing Lead-Lag Oscillations by a Mass-Spring-Damper Model

A simple mass-spring-damper model, shown in Figure 1, was suggested by SAE to be used for the torsional stability analysis of a rotor/engine system [13]. For an approximately rigid transmission shaft between the engine and the rotor hub, the model is further simplified as shown in Figure 3.

The dynamics, expressed in state equation form, is

$$\begin{bmatrix}\dot{\psi}_b\\ \dot{\Omega}_b\\ \dot{\psi}_{mr}\\ \dot{\Omega}_{mr}\end{bmatrix} = \begin{bmatrix}0 & 1 & 0 & 0\\ -\frac{k_l}{I_{z_Q}} & -\frac{b_l}{I_{z_Q}} & \frac{k_l}{I_{z_Q}} & \frac{b_l}{I_{z_Q}}\\ 0 & 0 & 0 & 1\\ \frac{k_l}{J_h} & \frac{b_l}{J_h} & -\frac{k_l}{J_h} & -\frac{b_l}{J_h}\end{bmatrix}\cdot \begin{bmatrix}\psi_b\\ \Omega_b\\ \psi_{mr}\\ \Omega_{mr}\end{bmatrix} + \begin{bmatrix}0\\0\\0\\ \frac{1}{J_h}\end{bmatrix} Q_{e_r}, \qquad (5)$$

where Ω_b is the angular speed of blade, and Ω_{mr} is the speed of main rotor hub.

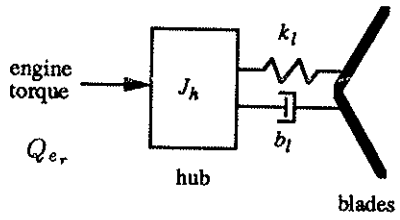

Figure 3: Generic Mass-Spring-Damper Model for Rotor/Engine Resonance Analysis

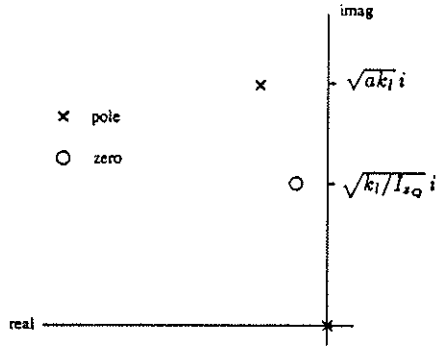

Figure 4: Poles and Zeros of $\Omega_{mr}(s)/Q_{e_r}(s)$

The transfer funstion from engine input torque to rotor speed is

$$\frac{\Omega_{mr}(s)}{Q_{e_r}(s)} = \frac{\left(s^2+b_l\,s/I_{z_Q}+k_l/I_{z_Q}\right)/J_h}{s\left(s^2+a\,b_l\,s+a\,k_l\right)}\,, \qquad (6)$$

where

$$a \equiv \frac{1}{J_h}+\frac{1}{I_{z_Q}}\,; \qquad (7)$$

and the poles and zeros of this transfer function are shown in Figure 4.

Let the lag angle be defined as

$$\xi \equiv \psi_{mr}-\psi_b\,; \qquad (8)$$

then Equation (5) can be rearranged, and ξ is decoupled from Ω_{mr} as shown below

$$\begin{bmatrix}\dot{\xi}\\ \ddot{\xi}\\ \dot{\Omega}_{mr}\end{bmatrix} = \begin{bmatrix}0 & 1 & 0\\ -\left(\frac{k_l}{I_{z_Q}}+\frac{k_l}{J_h}\right) & -\left(\frac{b_l}{I_{z_Q}}+\frac{b_l}{J_h}\right) & 0\\ -\frac{k_l}{J_h} & -\frac{b_l}{J_h} & 0\end{bmatrix}\cdot\begin{bmatrix}\xi\\ \dot{\xi}\\ \Omega_{mr}\end{bmatrix}+\begin{bmatrix}0\\0\\ \frac{Q_{e_r}}{J_h}\end{bmatrix}. \qquad (9)$$

Equation (9) agrees with the results of the previous section that coupling increases damping and frequency. However, if we compare this equation with

Model Type	Flexible Mode
Truth Model	-2.02 $\pm$ 12.07 i
Generic Model	-1.79 $\pm$ 11.56 i
Proposed Model	-1.90 $\pm$ 11.54 i

Table 2: Comparison of Natural Modes for Three Models of a Hypothetical One-Bladed Rotor

those in Section 4.1, we see that the missing coupling term between $\dot{\xi}$ and Ω_{mr}, and that the missing hub speed damping term are related to $2mey_g R^2 \Omega_{mr_0} \xi_0$ and $(\partial D/\partial \Omega_{mr})_0$, which are the sensitivity of the hub torque (due to centrifugal force) with respect to hub speed, and the aerodynamic damping, respectively. These effects are missing in the mass-spring-damper model.

4.3 Improved Mass-Spring-Damper Model

Adding an extra damping[1] b_h/J_h for hub speed (Ω_{mr}) to Equation (9), the coupled hub-blade equation becomes

$$\begin{bmatrix} \dot{\xi} \\ \ddot{\xi} \\ \dot{\Omega}_{mr} \end{bmatrix} \approx \begin{bmatrix} 0 & 1 \\ -\left(\frac{k_l}{I_{z_Q}} + \frac{k_l}{J_h}\right) & -\left(\frac{b_l}{I_{z_Q}} + \frac{b_l}{J_h}\right) \\ -\frac{k_l}{J_h} & -\frac{b_l}{J_h} \end{bmatrix} \begin{bmatrix} 0 \\ -\frac{b_h}{J_h} \\ -\frac{b_h}{J_h} \end{bmatrix} \begin{bmatrix} \xi \\ \dot{\xi} \\ \Omega_{mr} \end{bmatrix} + \begin{bmatrix} 0 \\ 0 \\ \frac{Q_{e_r}}{J_h} \end{bmatrix}, \quad (10)$$

where $b_h \equiv h_\omega$ (defined in Appendix A.2) approximates the aerodynamic damping.

Expressing the equation in terms of blade absolute angle (ψ_b), we get

$$\begin{bmatrix} \dot{\psi}_b \\ \dot{\Omega}_b \\ \dot{\psi}_{mr} \\ \dot{\Omega}_{mr} \end{bmatrix} \approx \begin{bmatrix} 0 & 1 & 0 \\ -\frac{k_l}{I_{z_Q}} & -\frac{b_l}{I_{z_Q}} & \frac{k_l}{I_{z_Q}} \\ 0 & 0 & 0 \\ \frac{k_l}{J_h} & \frac{b_l}{J_h} & -\frac{k_l}{J_h} \end{bmatrix} \begin{bmatrix} 0 \\ \frac{b_l}{I_{z_Q}} \\ 1 \\ -\left(\frac{b_l}{J_h} + \boxed{\frac{b_h}{J_h}}\right) \end{bmatrix} \begin{bmatrix} \psi_b \\ \Omega_b \\ \psi_{mr} \\ \Omega_{mr} \end{bmatrix} + \begin{bmatrix} 0 \\ 0 \\ 0 \\ \frac{Q_{e_r}}{J_h} \end{bmatrix} \quad (11)$$

The proposed modification for the model is shown in Figure 5.

If we consider the blade model in Figure 2 a truth model, then the natural modes for the truth model are compared with those of the spring-damper models in Table 2.

[1] The extra damping terms are suggested by Equations (2) and (3).

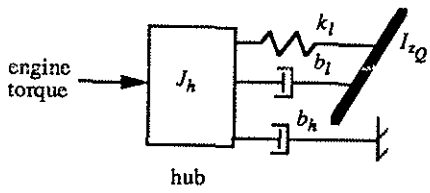

Figure 5: Proposed Mass-Spring-Damper Model for One-Bladed Rotor

5 Derivation of Coupled Flap-Lag Equations with Rotor Speed DOF

In the previous section, only the lead-lag motion of a hinged blade was considered. We found that the lead-lag motion has a strong effect on rotor load torque. Another blade DOF is the flap motion, which strongly affects rotor thrust and moments.

The flap and lead-lag motions of a blade are coupled. The coupled flap and lead-lag equations, for the i-th blade, at a constant rotor speed are [3] :

$$I_{x_Q}\, \delta\ddot{\beta}_i + \left(I_{x_Q} + m_i e y_g R^2\right) \Omega_{mr_0}^2\, \delta\beta_i = -\delta M_{aero_i}\,, \quad (12)$$

$$I_{z_Q}\, \delta\ddot{\xi}_i + b_{lh}\, \delta\dot{\xi}_i + m_i e y_g R^2 \Omega_{mr_0}^2\, \delta\xi_i - 2 I_{z_Q} \Omega_{mr_0} \dot{\beta}_{i_0}\, \delta\beta_i = -\delta N_{aero_i}\,, \quad (13)$$

where M_{aero_i} and N_{aero_i} are the moments created by aerodynamic forces, and where control moments are not included. These equations are accurate to second order small effects.

Figure 5 shows a blade creating both flap and lead-lag displacements. Two coordinate systems are shown with "s" defined as the shaft axis system, which is rotating with the shaft and is fixed at the hub, O; the "B" coordinates represent a blade body axis system, which is rotating with the blade and is fixed at the hinge, Q. The flap angle, β, the lead-lag angle, ξ, and the blade azimuth angle ψ, are shown poistive in the figure. Subscript "i" marks the ith blade.

Equations (12) and (13) represent the linearized flap and lead-lag dynamics that have been commonly used in rotor dynamics analysis. We like to extend these equations to include rotor speed variations. We are also interested in knowing whether the rotor speed DOF affects the blade flap-lag coupling. The derivation is based on the following assumptions :

- Rigid blades.
- Linear lead-lag dampers.

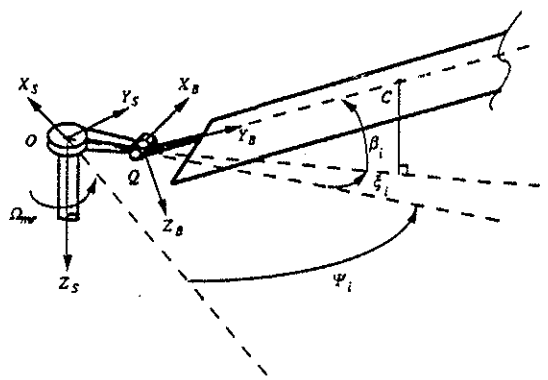

Figure 6: A Hinged Blade Undertaking Flap and Lead-Lag Motions

- Flap hinge and lead-lag hinge coincide.
- No kinematic coupling.
- No pre-cone angle.

Applying Lagrange's Equations, we get the flap equation of motion

$$I_{x_Q}\ddot{\beta}_i + I_{x_Q}\left(\dot{\psi}_i + \dot{\xi}_i\right)^2 c_{\beta_i}s_{\beta_i} + m_i e y_g R^2 \dot{\psi}_i^2 s_{\beta_i} c_{\xi_i} - m_i e y_g R^2 \ddot{\psi}_i s_{\beta_i} s_{\xi_i} + m_i g y_g R c_{\beta_i} = -M_{ext_i} , \quad (14)$$

where $I_{z_Q} = I_z + m y_g^2 R^2$ and $I_{x_Q} = I_x + m y_g^2 R^2$ represent the blade moments of inertia about the hinge. M_{ext_i} is the moment created by all external forces about flap hinge axis (including the control moment), and is positive in the $\mathbf{i}_B$ direction.

The lead-lag equation of motion is

$$I_{z_Q}\left(\ddot{\psi}_i + \ddot{\xi}_i\right) c_{\beta_i}^2 - 2I_{x_Q}\dot{\beta}_i\left(\dot{\psi}_i + \dot{\xi}_i\right) c_{\beta_i}s_{\beta_i} + I_y\left(\ddot{\psi}_i + \ddot{\xi}_i\right) s_{\beta_i}^2 + b_{lh}\dot{\xi}_i + m_i e y_g R^2 \ddot{\psi}_i c_{\beta_i} c_{\xi_i} + m_i e y_g R^2 \dot{\psi}_i^2 c_{\beta_i} s_{\xi_i} = -N_{ext_i} , \quad (15)$$

where N_{ext_i} is the external moment about lag hinge axis, positive in the $\mathbf{k}_B$; and b_{lh}, is the equivalent lag damper coefficient.

To linearize the flap and the lead-lag equations for small angles of β_i and ξ_i, we define

$$\beta_i = \beta_{i_0} + \delta\beta_i , \quad (16)$$
$$\xi_i = \xi_{i_0} + \delta\xi_i , \quad (17)$$
$$\Omega_{mr} = \dot{\psi}_i = \Omega_{mr_0} + \delta\Omega_{mr} , \quad (18)$$
$$\dot{\Omega}_{mr} = \ddot{\psi}_i = \delta\dot{\Omega}_{mr} . \quad (19)$$

Substitute Equations (16) to (19) into (14) and (15), and make small angle approximations for β_{i_0} and ξ_{i_0}. After dropping small terms of the third- and higher-orders, the flap equation becomes

$$I_{x_Q}\delta\ddot{\beta}_i + \left(I_{x_Q} + m_i e y_g R^2\right)\Omega_{mr_0}^2\delta\beta_i + 2\left(I_{x_Q} + m_i e y_g R^2\right)\Omega_{mr_0}\beta_{i_0}\delta\Omega_{mr} + 2I_{x_Q}\Omega_{mr_0}\beta_{i_0}\delta\dot{\xi}_i = -\delta M_{ext_i} , \quad (20)$$

and the lead-lag equation becomes

$$I_{z_Q}\delta\ddot{\xi}_i + b_{lh}\delta\dot{\xi}_i + m_i e y_g R^2\Omega_{mr_0}^2\delta\xi_i + 2m_i e y_g R^2\Omega_{mr_0}\xi_{i_0}\delta\Omega_{mr} - 2I_{x_Q}\Omega_{mr_0}\left(\dot{\beta}_{i_0}\delta\beta_i + \beta_{i_0}\delta\dot{\beta}_i + \delta\dot{\beta}_i\delta\beta_i\right) = -\delta N_{ext_i} + \left(I_{x_Q} + m_i e y_g R^2\right) . \quad (21)$$

Finally, if we retain only the most significant second-order terms, the flap equation simplifies to

$$I_{x_Q}\delta\ddot{\beta}_i + \left(I_{x_Q} + m_i e y_g R^2\right)\Omega_{mr_0}^2\delta\beta_i = -\delta M_{ext_i} . \quad (22)$$

Similarly, the lead-lag equation, with $I_x \approx I_z$ for a large aspect ratio blade, simplifies to

$$I_{z_Q}\delta\ddot{\xi}_i + b_{lh}\delta\dot{\xi}_i + m_i e y_g R^2\Omega_{mr_0}^2\delta\xi_i - 2I_{z_Q}\Omega_{mr_0}\dot{\beta}_{i_0}\delta\beta_i = -\delta N_{ext_i} + \left(I_{z_Q} + m_i e y_g R^2\right)\left(-\dot{\Omega}_{mr}\right) . \quad (23)$$

From Equation (20) we conclude that *the shaft angular acceleration does not affect flapping dynamics, and that the only significant coupling between the flap and lead-lag motions is the Coriolis force,* $2I_{x_Q}\Omega_{mr_0}\dot{\beta}_{i_0}\delta\beta_i$ (in Equation 23).

Also in Equation (23), the shaft angular acceleration ($\dot{\Omega}_{mr} \neq 0$) directly excites the lead-lag motion; hence, a decelerating rotor ($\dot{\Omega}_{mr} < 0$) acts to increase the lead angles.

6 Flap and Lead-Lag Equations in Multiblade Coordinates

The coupled flap and lead-lag equations of Section 5 are transformed into multiblade coordinates (cf. [7] and [9]) for a rotor operating near hover condition. Let $\underline{\beta}_{nr}$ and $\underline{\xi}_{nr}$ be the state vectors of flap and lead-lag DOF's in the multiblade coordinates, and let the transformation matrix be $\mathbf{T}_{mb}$. Then for flapping dynamics, Equation (22), is transformed into

$$\delta\ddot{\underline{\beta}}_{nr} + \mathbf{T}_{mb}^T\left(2\dot{\mathbf{T}}_{mb} + \overline{d}_f\,\mathbf{T}_{mb}\right)\delta\dot{\underline{\beta}}_{nr} + \mathbf{T}_{mb}^T\left(\ddot{\mathbf{T}}_{mb} + \overline{d}_f\,\dot{\mathbf{T}}_{mb} + \overline{\nu}_f^2\,\mathbf{T}_{mb}\right)\delta\underline{\beta}_{nr} = -\frac{1}{I_{x_Q}}\mathbf{T}_{mb}^T\left(\frac{\partial M}{\partial \underline{u}_r}\right)_0^T \underline{u}_r , \quad (24)$$

where $m \equiv m_i$ and

$$\overline{d}_f \equiv \frac{1}{I_{x_Q}}\left(\frac{\partial M}{\partial \dot{\beta}_i}\right)_0 , \quad (25)$$

$$\overline{\nu}_f^2 \equiv \left(1 + \frac{m e y_g R^2}{I_{x_Q}}\right)\Omega_{mr_0}^2 + \frac{1}{I_{x_Q}}\left(\frac{\partial M}{\partial \beta_i}\right)_0 \quad (26)$$

The flap dynamics in the multiblade coordinates is again decoupled from the lead-lag dynamics. So for rotor/engine torsional dynamics analysis, the flap motion is like an input disturbance.

For lead-lag dynamics, the rotor angular acceleration ($\dot{\Omega}_{mr}$) in Equation (23) is first eliminated. The angular acceleration can be expressed as a function of blade state (see Equations (3)) and input variables, i. e.,

$$\dot{\Omega}_{mr} = \sum_{i=1}^{n_b}(f_{\dot{\omega}\beta_i}\,\delta\beta_i + f_{\dot{\omega}\dot{\beta}_i}\,\delta\dot{\beta}_i + f_{\dot{\omega}\xi_i}\,\delta\xi_i + f_{\dot{\omega}\dot{\xi}_i}\,\delta\dot{\xi}_i) + f_{\dot{\omega}\omega}\,\delta\Omega_{mr} + G_{\dot{\omega}r}\,\underline{u}_r + d_2\,\delta Q_{e_r} \quad (27)$$

where

$$f_{\dot{\omega}\beta_i} \equiv -d_2\left(\frac{\partial Q_r}{\partial \beta_i}\right)_0 , \quad (28)$$

$$f_{\dot{\omega}\dot{\beta}_i} \equiv -d_2\left(\frac{\partial Q_r}{\partial \dot{\beta}_i}\right)_0 , \quad (29)$$

$$f_{\dot{\omega}\xi_i} \equiv \underbrace{-d_2\left(\frac{\partial Q_r}{\partial \xi_i}\right)_0}_{<0} , \quad (30)$$

$$f_{\dot{\omega}\dot{\xi}_i} \equiv \underbrace{-d_2\left(\frac{\partial Q_r}{\partial \dot{\xi}_i}\right)_0}_{<0} , \quad (31)$$

$$f_{\dot{\omega}\omega} \equiv -d_2 h_\omega , \quad (32)$$

$$G_{\dot{\omega}r} \equiv -d_2\left(\frac{\partial Q_r}{\partial \underline{x}_r}\right)_0^T ; \quad (33)$$

and where $d_2 \equiv 1/\left[J_h + \left(\partial Q_r/\partial\dot{\Omega}_{mr}\right)_0\right]$, Q_{e_r} is the engine torque, and Q_r is the load torque of main and tail rotors. The coefficients defined in Equations (28) through (31) are same for all blade in hover.

So the lead-lag equations for all n_b blades in the blade rotating coordinates are

$$\begin{aligned}\delta\ddot{\underline{\xi}}_r + \overline{d}_l\,\delta\dot{\underline{\xi}}_r + \overline{\nu}_l^2\,\delta\underline{\xi}_r + c_1 f_{\dot{\omega}\dot{\xi}}\,P\,\delta\dot{\underline{\xi}}_r + c_1 f_{\dot{\omega}\xi}\,P\,\delta\underline{\xi}_r \\ = \left(\overline{f}_{l\beta}\,\mathbf{I} - c_1 f_{\dot{\omega}\beta}\,P\right)\delta\underline{\beta}_r + \\ \left(\overline{f}_{l\dot{\beta}}\,\mathbf{I} - c_1 f_{\dot{\omega}\dot{\beta}}\,P\right)\delta\dot{\underline{\beta}}_r - c_1 f_{\dot{\omega}\omega}\,\mathbf{I}\,\delta\Omega_{mr} - \\ \left[c_1\,G_{\dot{\omega}r} + \frac{1}{I_{z_Q}}\left(\frac{\partial N}{\partial \underline{u}_r}\right)_0^T\right]\mathbf{I}\,\underline{u}_r - \\ c_1\,d_2\,\mathbf{I}\,\delta Q_{e_r} , \end{aligned} \quad (34)$$

where $\overline{d}_l$, $\overline{\nu}_l$, $\overline{f}_{l\beta}$, and $\overline{f}_{l\dot{\beta}}$ are

$$\overline{d}_l \equiv \frac{b_{lh}}{I_{z_Q}} + \frac{1}{I_{z_Q}}\left(\frac{\partial N}{\partial \dot{\xi}_i}\right)_0 , \quad (35)$$

$$\overline{\nu}_l^2 \equiv \frac{m_i e y_g R^2 \Omega_{mr_0}^2}{I_{z_Q}} + \frac{1}{I_{z_Q}}\left(\frac{\partial N}{\partial \xi_i}\right)_0 , \quad (36)$$

$$\overline{f}_{l\beta} \equiv 2\Omega_{mr_0}\dot{\beta}_{i_0} - \frac{1}{I_{z_Q}}\left(\frac{\partial N}{\partial \beta_i}\right)_0 , \quad (37)$$

$$\overline{f}_{l\dot{\beta}} \equiv -\frac{1}{I_{z_Q}}\left(\frac{\partial N}{\partial \dot{\beta}_i}\right)_0 ; \quad (38)$$

with

$$\begin{aligned}\delta N_{ext_i} \approx \left(\frac{\partial N}{\partial \beta_i}\right)_0\delta\beta_i + \left(\frac{\partial N}{\partial \dot{\beta}_i}\right)_0\delta\dot{\beta}_i + \\ \left(\frac{\partial N}{\partial \xi_i}\right)_0\delta\xi_i + \left(\frac{\partial N}{\partial \dot{\xi}_i}\right)_0\delta\dot{\xi}_i + \\ \left(\frac{\partial N}{\partial \underline{u}_r}\right)_0^T\underline{u}_r . \end{aligned} \quad (39)$$

Furthermore, c_1 is as in Equation (102); and for a four-bladed rotor,

$$P \equiv \begin{bmatrix} 1 & 1 & 1 & 1 \\ 1 & 1 & 1 & 1 \\ 1 & 1 & 1 & 1 \\ 1 & 1 & 1 & 1 \end{bmatrix} . \quad (40)$$

The last two terms of the left hand side of Equation (34) are transformed to the multiblade coordinates as follows :

$$\begin{aligned} c_1 f_{\dot{\omega}\xi} P\,\delta\underline{\xi}_r &= c_1 f_{\dot{\omega}\xi} P\mathbf{T}_{mb}\,\delta\underline{\xi}_{nr} \\ &= c_1 f_{\dot{\omega}\xi}\underbrace{\begin{bmatrix} 4 & 0 & 0 & 0 \\ 4 & 0 & 0 & 0 \\ 4 & 0 & 0 & 0 \\ 4 & 0 & 0 & 0 \end{bmatrix}}_{\mathbf{T}_1}\delta\underline{\xi}_{nr} , \end{aligned} \quad (41)$$

$$\begin{aligned} c_1 f_{\dot{\omega}\dot{\xi}} P\,\delta\dot{\underline{\xi}}_r &= c_1 f_{\dot{\omega}\dot{\xi}}\underbrace{P\dot{\mathbf{T}}_{mb}}_{\mathbf{0}}\delta\underline{\xi}_{nr} + \\ &\quad c_1 f_{\dot{\omega}\dot{\xi}}\underbrace{P\mathbf{T}_{mb}}_{\mathbf{T}_1}\delta\dot{\underline{\xi}}_{nr} , \\ &= c_1 f_{\dot{\omega}\dot{\xi}}\mathbf{T}_1\,\delta\dot{\underline{\xi}}_{nr} ; \end{aligned} \quad (42)$$

Using Equations (41), (42), the multiblade lead-lag equations are

$$\begin{aligned}\delta\ddot{\underline{\xi}}_{nr} + \mathbf{T}_{mb}^T\left(2\dot{\mathbf{T}}_{mb} + \overline{d}_l\mathbf{T}_{mb} + \boxed{c_1 f_{\dot{\omega}\dot{\xi}}\mathbf{T}_1}\right)\delta\dot{\underline{\xi}}_{nr} + \\ \mathbf{T}_{mb}^T\left(\ddot{\mathbf{T}}_{mb} + \overline{d}_l\dot{\mathbf{T}}_{mb} + \overline{\nu}_l^2\mathbf{T}_{mb} + \boxed{c_1 f_{\dot{\omega}\xi}\mathbf{T}_1}\right)\cdot \\ \delta\underline{\xi}_{nr} = R.H.S. , \end{aligned} \quad (43)$$

and the right hand side ($R.H.S.$) is given by

$$\begin{aligned} R.H.S. = \mathbf{T}_{mb}^T[\left(\overline{f}_{l\beta}\,\mathbf{I} - c_1 f_{\dot{\omega}\beta}\,P\right)\mathbf{T}_{mb} + \\ \left(\overline{f}_{l\dot{\beta}}\,\mathbf{I} - c_1 f_{\dot{\omega}\dot{\beta}}\,P\right)\dot{\mathbf{T}}_{mb}]\delta\underline{\beta}_{nr} + \\ \mathbf{T}_{mb}^T\left(\overline{f}_{l\dot{\beta}}\,\mathbf{I} - c_1 f_{\dot{\omega}\dot{\beta}}\,P\right)\mathbf{T}_{mb}\,\delta\dot{\underline{\beta}}_{nr} - \\ c_1 f_{\dot{\omega}\omega}\,\mathbf{T}_{mb}^T\,\delta\Omega_{mr} - \\ \mathbf{T}_{mb}^T\left[c_1\,G_{\dot{\omega}r} + \frac{1}{I_{z_Q}}\left(\frac{\partial N}{\partial \underline{u}_r}\right)_0^T\right]\underline{u}_r - \\ c_1\,d_2\,\mathbf{I}\,\delta Q_{e_r} . \end{aligned} \quad (44)$$

The boxed terms in Equation (43) confirm the results of increased lead-lag damping and natural frequency due to hub-blade coupling. After substituting $\mathbf{T}_1$ in those terms, we see that *only the collective*

mode (the smallest frequency mode), ξ_0, is affected by the shaft DOF. The progressive and regressive lead-lag modes are not affected. This suggests that only the collective lead-lag oscillation needs to be considered in the analysis of torsional resonance near hover.

6.1 An Example of Multiblade Lead-Lag Equations with Shaft DOF

A simplified, three-bladed rotor[2] is used in this example to show the changes of rotor lead-lag eigenvalues with variable rotor speeds. Each blade has one DOF, and possesses the same properties as those defined in Section 4.

Since the large centrifugal force on each blade keeps its lag angle small, the lead-lag equation for the i-th blade is approximated by Equation (100) :

$$\ddot{\xi}_i + d_l' \dot{\xi}_i + \nu_l^2 \xi_i \approx c_1 \dot{\Omega}_{mr} , \tag{45}$$

where

$$d_l' \equiv \frac{1}{I_{z_Q}} \left[b_{lh} - y_g R \left(\frac{\partial D}{\partial \dot{\xi}_i} \right)_0 \right] , \tag{46}$$

$$\nu_l^2 \equiv \frac{m e y_g R^2}{I_{z_Q}} \Omega_{mr_0}^2 . \tag{47}$$

The variation in rotor load torque for just one blade is given by Equation (94); so for three blades, the load variation is

$$\delta Q_{mr} \approx eRq_1 \Omega_{mr_0}^2 \sum_{k=1}^{3} \delta\xi_k + eRq_2'' \sum_{k=1}^{3} \delta\dot{\xi}_k + 3h_\omega \, \delta\Omega_{mr} + 3eRq_4 \, \dot{\Omega}_{mr} . \tag{48}$$

The linearized equations for rotor angular acceleration as well as lead-lag dynamics are therefore

$$\dot{\Omega}_{mr} + b_\omega \, \delta\Omega_{mr} \approx -\lambda \sum_{k=1}^{3} \delta\xi_k - \mu \sum_{k=1}^{3} \delta\dot{\xi}_k + d_3 \, \delta Q_{e_r} , \tag{49}$$

$$\delta\ddot{\xi}_i + d_l' \, \delta\dot{\xi}_i + \nu_l^2 \, \delta\xi_i + c_1 \mu \sum_{k=1}^{3} \delta\dot{\xi}_k + c_1 \lambda \sum_{k=1}^{3} \delta\xi_k \approx -c_1 b_\omega \, \delta\Omega_{mr} + c_1 d_3 \, \delta Q_{e_r} , \tag{50}$$

where

$$d_3 \equiv \frac{1}{J_h + 3eRq_4} , \tag{51}$$

$$b_\omega \equiv 3 d_3 \, h_\omega , \tag{52}$$

$$\lambda \equiv d_3 eRq_1 \Omega_{mr_0}^2 , \tag{53}$$

$$\mu \equiv d_3 eRq_2'' . \tag{54}$$

[2] Although the transformed equations in the previous section were derived for a four-bladed rotor, using a three-bladed rotor here as an example is sufficient to demonstrate the point. The lead-lag dynamics for a four-bladed rotor in multiblade coordinates contain one reactionless (differential) mode.

Assume $e \ll 1$, and that perfect symmetry exists in all three blades, i. e., $\xi_1 = \xi_2 = \xi_3$. So $c_1 \approx 1$ and Equations (50) and (49) are simplified to

$$\delta\ddot{\xi}_i + (d_l' + 3\mu) \, \delta\dot{\xi}_i + (\nu_l^2 + 3\lambda) \, \delta\xi_i \approx -b_\omega \, \delta\Omega_{mr} + d_3 \, \delta Q_{e_r} , \tag{55}$$

$$\dot{\Omega}_{mr} + b_\omega \, \delta\Omega_{mr} \approx -3\lambda \, \delta\xi_i - 3\mu \, \delta\dot{\xi}_i + d_3 \, \delta Q_{e_r} . \tag{56}$$

The transfer function from δQ_{e_r} to $\delta\Omega_{mr}$ is found from Equations (55) and (56) as

$$\frac{\delta\Omega_{mr}(s)}{\delta Q_{e_r}(s)} = \frac{d_3 \left(s^2 + d_l' s + \nu_l^2 \right)}{(s + b_\omega)(s^2 + d_l' s + \nu_l^2) + 3s(\lambda + \mu s)} . \tag{57}$$

The characteristic equation, after substituting the expressions for λ and μ, is rearranged to extract the lead-lag damper coefficient (b_{lh}), and the aerodynamic damping ($b_a \equiv \partial D / \partial \dot{\xi}$) explicitly. The final expression is approximated by

$$(s + b_\omega)(s^2 + \nu_l^2) + 3\lambda s + b_a \, s(a_1 \, s + a_2) + b_{lh} \, s(a_3 \, s + a_4) \approx 0 , \tag{58}$$

where

$$a_1 \equiv 3 d_3 eRq_3 - \frac{y_g R}{I_{z_Q}} , \tag{59}$$

$$a_2 \equiv -\frac{b_\omega y_g R}{I_{z_Q}} , \tag{60}$$

$$a_3 \equiv 3 d_3 \left(1 + \frac{m e y_g R^2}{I_{z_Q}} \right) + \frac{1}{I_{z_Q}} , \tag{61}$$

$$a_4 \equiv \frac{b_\omega}{I_{z_Q}} . \tag{62}$$

The roots of the characteristic equation can be thought of functions of three design parameters, λ, b_a, and b_{lh}, of which the first two parameters are fixed for a given blade geometry and mass property, and the third parameter is to be chosen during the design process to assure rotor stability.

The roots of the lead-lag equation are analyzed using the Root Locus technique, and are shown in Figures 7.

To describe the dynamics of the entire rotor, individual blade lead-lag dyanmic equations are transformed into multiblade equations. A scaled transformation matrix, $\mathbf{T}_{mb}$, for a three-bladed rotor is given by (cf. [4])

$$\underbrace{\begin{bmatrix} \delta\xi_1 \\ \delta\xi_2 \\ \delta\xi_3 \end{bmatrix}}_{\delta\underline{\xi}_r} \equiv \begin{bmatrix} \frac{1}{\sqrt{3}} & \sqrt{\frac{2}{3}} c_{\psi_1} & \sqrt{\frac{2}{3}} s_{\psi_1} \\ \frac{1}{\sqrt{3}} & \sqrt{\frac{2}{3}} c_{\psi_2} & \sqrt{\frac{2}{3}} s_{\psi_2} \\ \frac{1}{\sqrt{3}} & \sqrt{\frac{2}{3}} c_{\psi_3} & \sqrt{\frac{2}{3}} s_{\psi_3} \end{bmatrix} \delta\underline{\xi}_{nr} , \tag{63}$$

where ψ_i is the azimuth angle of the ith blade, $\delta\underline{\xi}_r$ represents the lag angles of three rotating blades, $\delta\underline{\xi}_{nr}$ represents the multiblade lag angles of the rotor : ξ_0,

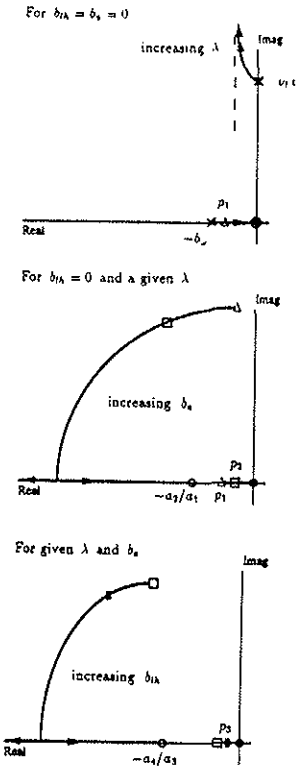

Figure 7: Open-Loop Poles of Simplified Three-Bladed Rotor

ξ_{1c}, and ξ_{1s} are the collective, longitudinal cyclic, and lateral cyclic angles, respectively.

Using the definition of the multiblade transformation in Equation (63), where the scaled transformation matrix $\mathbf{T}_{mb}$ is orthogonal, the lead-lag dynamics in rotating blade coordinates is tranformed into nonrotating, multiblade coordinates as follows:

$$\delta\ddot{\underline{\xi}}_{nr} + \mathbf{T}_{mb}^T \left(2\dot{\mathbf{T}}_{mb} + d_l'\mathbf{T}_{mb} + c_1\mu\mathbf{U}\right) \delta\dot{\underline{\xi}}_{nr} + \mathbf{T}_{mb}^T \left(\ddot{\mathbf{T}}_{mb} + d_l'\dot{\mathbf{T}}_{mb} + \nu_l^2\mathbf{T}_{mb} + c_1\lambda\mathbf{U}\right) \delta\underline{\xi}_{nr} \approx \begin{bmatrix} \sqrt{3} \\ 0 \\ 0 \end{bmatrix} (-b_\omega\,\delta\Omega_{mr} + d_3\,\delta Q_{e_r}), \quad (64)$$

where $\mathbf{U} \equiv \begin{bmatrix} \sqrt{3} & 0 & 0 \\ \sqrt{3} & 0 & 0 \\ \sqrt{3} & 0 & 0 \end{bmatrix}$.

Further reduction of Equation (64) yields

$$\delta\ddot{\underline{\xi}}_{nr} + \begin{bmatrix} d_l' + 3c_1\mu & 0 & 0 \\ 0 & d_l' & 2\Omega_{mr_0} \\ 0 & -2\Omega_{mr_0} & d_l' \end{bmatrix} \delta\dot{\underline{\xi}}_{nr} + \begin{bmatrix} \nu_l^2 + 3c_1\lambda & 0 & 0 \\ 0 & \nu_l^2 - \Omega_{mr_0}^2 & d_l'\Omega_{mr_0} \\ 0 & -d_l'\Omega_{mr_0} & \nu_l^2 - \Omega_{mr_0}^2 \end{bmatrix} \delta\underline{\xi}_{nr} = \begin{bmatrix} g_1 \\ 0 \\ 0 \end{bmatrix} \delta\Omega_{mr} + \begin{bmatrix} g_2 \\ 0 \\ 0 \end{bmatrix} d_3\,\delta Q_{e_r}, \quad (65)$$

where

$$g_1 \equiv \sqrt{3}(-c_1 b_\omega), \quad (66)$$

$$g_2 \equiv \sqrt{3}. \quad (67)$$

Similarly, the shaft dynamics is given by

$$\dot{\Omega}_{mr} = \delta\dot{\Omega}_{mr} = d_3\,\delta Q_{e_r} - b_\omega\,\delta\Omega_{mr} - \lambda\,\mathbf{P}_1\,\delta\underline{\xi}_{nr} - \mu\,\mathbf{P}_1\,\delta\dot{\underline{\xi}}_{nr}, \quad (68)$$

where $\mathbf{P}_1 \equiv [\sqrt{3},\, 0,\, 0]$.

Take the Laplace transform of Equations (65) and (68), the combined rotor and shaft dynamics for multiblade lead-lag state variables becomes

$$\begin{bmatrix} s^2 + \overline{d}_l\,s + \overline{\nu}_l^2 & 0 & 0 & -g_1 \\ 0 & p_1(s) & p_2(s) & 0 \\ 0 & -p_2(s) & p_1(s) & 0 \\ \sqrt{3}\,(\mu\,s + \lambda) & 0 & 0 & s + b_\omega \end{bmatrix} \cdot \begin{bmatrix} \delta\xi_0(s) \\ \delta\xi_{1c}(s) \\ \delta\xi_{1s}(s) \\ \delta\Omega(s) \end{bmatrix} = \begin{bmatrix} g_2 \\ 0 \\ 0 \\ 1 \end{bmatrix} d_3\,\delta Q_{e_r}, \quad (69)$$

where

$$\overline{d}_l \equiv d_l' + 3c_1\,\mu, \quad (70)$$

$$\overline{\nu}_l^2 \equiv \nu_l^2 + 3c_1\,\lambda, \quad (71)$$

$$p_1(s) \equiv s^2 + d_l'\,s + \left(\nu_l^2 - \Omega_{mr_0}^2\right), \quad (72)$$

$$p_2(s) \equiv \Omega_{mr_0}\,(2s + d_l'). \quad (73)$$

Using this simplified rotor, we demonstrated that the rotor speed DOF only affects the collective lead-lag mode. The lead-lag mode and the rotor speed mode are coupled. The transfer function from engine torque to rotor speed is given by

$$\frac{\delta\Omega(s)}{\delta Q_{e_r}(s)} = \frac{d_3\left(s^2 + d_l'\,s + \nu_l^2\right)}{q(s)}, \quad (74)$$

where

$$q(s) \equiv (s + b_\omega)\left(s^2 + \overline{d}_l\,s + \overline{\nu}_l^2\right) + \sqrt{3}g_1\,(\mu\,s + \lambda). \quad (75)$$

The characteristic equation is exactly the same as that of Equation (57), if $e \ll 1$, or $c_1 \approx 1$; therefore, the results about pole locations for an individual blade apply directly to the dynamics of the entire rotor (in terms of the collective lag angle).

7 Further Improvement for Spring-Damper Model

An articulated rotor usually contains at least three blades. To analyze the torsional resonance for a multiblade rotor using the mass-spring-damper model, an immediate question arises : how to characterize the

Model Type	Flexible Mode
Truth Model	-4.17 ± 17.6 i
Generic Model	-1.79 ± 20.18 i
Proposed Model	-4.28 ± 16.47 i

Table 3: Comparison of Natural Modes for Three Models of a Three-Bladed Rotor

cumulative effects of all blades in this model? A common approach is to add the centrifugal spring constants from all blades, but a cumulative damper coefficient is usually not used in the analysis. However, from the three-bladed rotor example, the additive effects for spring and damper only went into the rotor angular acceleration equation, where the rotor torque was computed as the sum of the torques produced by individual blades. So for a three-bladed rotor, the hub-blade dynamics is modified from Equation (11) as

$$\begin{bmatrix} \dot{\psi}_b \\ \dot{\Omega}_b \\ \dot{\psi}_{mr} \\ \dot{\Omega}_{mr} \end{bmatrix} \approx \begin{bmatrix} 0 & 1 & 0 \\ -\frac{k_l}{I_{z_Q}} & -\frac{b_l}{I_{z_Q}} & \frac{k_l}{I_{z_Q}} \\ 0 & 0 & 0 \\ \frac{3k_l}{J_h} & \frac{3b_l}{J_h} & -\frac{3k_l}{J_h} \end{bmatrix} \begin{bmatrix} \psi_b \\ \Omega_b \\ \psi_{mr} \\ \Omega_{mr} \end{bmatrix} + \begin{bmatrix} 0 \\ 0 \\ 0 \\ \frac{Q_{e_r}}{J_h} \end{bmatrix} \begin{bmatrix} 0 \\ \frac{b_l}{I_{z_Q}} \\ 1 \\ -3\left(\frac{b_l}{J_h} + \frac{b_h}{J_h}\right) \end{bmatrix} \quad (76)$$

where "3" can be replaced by the number of blades (n_B) if it is other than three.

Note in this equation that blade lead-lag motion is still characterized by the original spring constant and damper coefficient. So only the coupling part is changed, but the blade oscillation itself is not. This effectively models the collective motion of the blades in a rotor, and it fits well with the finding that only the collective lead-lag motion needs to be considered in torsional resonance studies.

If a cumulative spring constant (sum of all blades) is used in the spring-damper model, the predicted resonant frequency is higher than the actual frequency. On the other hand, since the cumulative effect of dampers is not considered in conventional analyses, the damping ratio of torsional modes are smaller. Figure 8 proposes an improvement to the spring-damper model; namely, to model individual blades explicitly.

Using the three-bladed rotor as an example, the natural modes of the truth model, the spring-damper model with cumulative spring constant and damper coefficient (Figure 8), and of the generic model are compared in Table 3. The predicted frequency for the generic model is 15 % higher, and the damping ratio is approximately 160 % less.

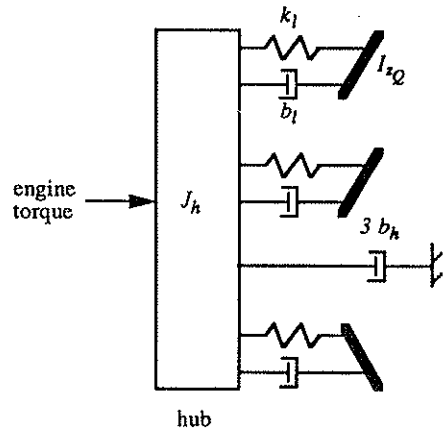

Figure 8: Proposed Mass-Spring-Damper Model for Three-Bladed Rotors

8 Simulations of Black Hawk Rotor System

The effects of the rotor speed DOF on rotor system natural modes are demonstrated for the simulated Black Hawk rotor system. This rotor system (ROTSIM) [8] simulates the main and tail rotors of the Sikorsky Black Hawk helicopter.

A series of linear models for the rotor system were generated with varying degrees of lag damping. The damper stiffness is selected as a parameter because it is a critical design factor for adequate torsional stability (the nonlinearity and the stiffness of lead-lag dampers were found to be factors inducing torque and speed oscillations).

Figure 9 shows the eigenvalues of the rotor in both the constant and variable rotor speed conditions. In the constant speed situation, the lead-lag modes become more damped for increasing amounts of lead-lag damper coefficient. The flap modes are not affected. When the rotor speed DOF is present, the collective lead-lag modes are shifted due to the coupling, and both the undamped natural frequency and the damping ratio are increased. Eventually, as the lead-lag damper gets stiff enough, collective lead-lag eigenvalues become two *real* values.

In the figure, the natural frequency of the collective lead-lag mode for a nominal value of damper coefficient is around 17 *rad/sec*. This frequency corresponds to the engine/rotor torsional oscillation, which is usually referred to as the first torsional mode. The frequency of the first torsional mode, for the Black Hawk type of helicopters, has been estimated to fall between 15 to 20 *rad/sec* (cf. [10] and [1]) using frequency sweeps on analog computer simulations. So the analysis of rotor/engine dynamics with rotor speed DOF in this research agrees with published simulation results.

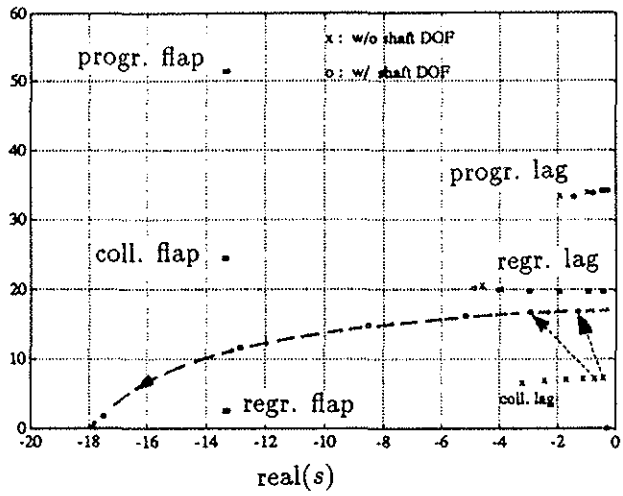

Figure 9: Rotor Eigenvalues for Varying Degrees of Lead-Lag Damping

9 Conclusion

Couplings between rotor and engine systems are represented by the rotor speed DOF. The effect of this DOF is to increase the damping ratio and natural frequency of a blade's lead-lag oscillations compared to a constant rotor speed model. In multiblade coordinates, the speed DOF affects only the collective lead-lag mode for a rotor near hover flight condition. The collective lead-lag mode, with this rotor speed DOF included, represents the first torsional mode of a combined rotor/engine system.

Torsional resonances can also be predicted by a simplified mass-spring-damper model. The generic spring-damper model was found inadequate; consequently, two improvements for this model were proposed which resulted in more accurate predictions of the resonance. This improved spring-damper model effectively models the collective lead-lag dynamics in a rotor/engine system.

10 Acknowledgement

The authors gratefully acknowledge two organizations for the support of this research. The Garrett Engine Division of Allied-Signal Aerospace Company provided financial support, and the Ames Research Center of NASA provided a Black Hawk helicopter simulation program.

A Derivations of Equations of Motion for a Hypothetical Rotor

The equations of motion for the hypothetical rotor shown in Figure 2 are derived in this section. First, the position vector of the center of mass (c.m., at point C) expressed in the blade body axes ($_B$) is

$$\mathbf{r}_C^B = eR\sin\xi\ \mathbf{i}_B + (e\cos\xi + y_g)\,R\,\mathbf{j}_B\,. \qquad (77)$$

The velocity of the c.m. is

$$\mathbf{v}_C^B = \left[(e\cos\xi + y_g)\,R\Omega_{mr} - y_g R\dot{\xi}\right]\mathbf{i}_B - eR\Omega_{mr}\sin\xi\ \mathbf{j}_B\,. \qquad (78)$$

Summing moments about the lead-lag hinge, Q, and making small angle approximations for ξ and $\dot{\xi}$, the equation of motion for the blade in the lead-lag DOF becomes

$$I_{z_Q}\ddot{\xi} + b_{lh}\dot{\xi} + mey_gR^2\Omega_{mr}^2\xi \approx y_gRD + \left(I_{z_Q} + mey_gR^2\right)\dot{\Omega}_{mr}\,, \qquad (79)$$

where $I_{z_Q} = I_{z_C} + my_g^2R^2$ is the blade moment of inertia about the hinge, b_{lh} is the equivalent lag damper coefficient.

The second term on the right hand side of Equation (79) results from rotor shaft rotational DOF. If we ignore this term ($\dot{\Omega}_{mr}$), then the natural frequency of blade lag motion, ν_l, would be (based on the blade properties of Table 1) $\sqrt{mey_gR^2\Omega_{mr}^2/I_{z_Q}} = 7.76$ *rad/sec*, which is slightly above 1/4 *per rev.*

A.1 Rotor Torque

The (load) torque, Q_{mr}, that the damper and the shear forces at lag hinge produce, is

$$Q_{mr} = eR(Y_Q\sin\xi - X_Q\cos\xi) + b_{lh}\dot{\xi}\,, \qquad (80)$$

where X_Q and Y_Q are the total shear forces that the blade exerts on the hinge. There are two types of shear forces at the hinge: *inertial* force and *aerodynamic* force. Summing these forces at the hinge, we get total shear forces in the blade body axes as follows :

$$X_Q = meR{\Omega_{mr}}^2\sin\xi - my_gR\left(\dot{\Omega}_{mr} - \ddot{\xi}\right) - meR\dot{\Omega}_{mr}\cos\xi - D\cos\theta_1\,, \qquad (81)$$

$$Y_Q = meR{\Omega_{mr}}^2\cos\xi + meR\dot{\Omega}_{mr}\sin\xi + my_gR\left(\Omega_{mr} - \dot{\xi}\right)^2 + D\sin\theta_1\,. \qquad (82)$$

For small ξ and $\dot{\xi}$, the angle θ_1 can be approximated by

$$\theta_1 \approx \frac{\xi}{1 + \frac{y_g}{e}}\ (<\xi)\,. \qquad (83)$$

So the load torque is approximated from Equations (79), (81), (82), and Equation(83) as

$$\begin{aligned} Q_{mr} &\approx eR(Y_Q\,\xi - X_Q) + b_{lh}\,\dot{\xi}\,, \\ &\approx eR(q_1\Omega_{mr}^2\,\xi + q_2\,\dot{\xi} + q_3 D + q_4\,\dot{\Omega}_{mr} + \\ &\quad q_5\,\Omega_{mr}\,\xi\dot{\xi})\,, \end{aligned} \tag{84}$$

where

$$\begin{aligned} q_1 &\equiv my_g R + \frac{m^2 e {y_g}^2 R^3}{I_{z_Q}}\,, \\ &= my_g R(1 + 3ey_g)\,, \end{aligned} \tag{85}$$

$$\begin{aligned} q_2 &\equiv b_{lh}\left(\frac{my_g R}{I_{z_Q}} + \frac{1}{eR}\right), \\ &= \frac{b_{lh}}{R}\left(3y_g + \frac{1}{e}\right), \end{aligned} \tag{86}$$

$$q_3 \equiv 1 - \frac{m{y_g}^2 R^2}{I_{z_Q}} = 1 - 3y_g^2\,, \tag{87}$$

$$q_4 \equiv meR - \frac{m^2 e {y_g}^2 R^3}{I_{z_Q}} = meRq_3\,, \tag{88}$$

$$q_5 \equiv -2my_g R\,. \tag{89}$$

The drag produced by this simple, rectangular blade can be estimated by blade element theory (cf. [14]). At zero lift, the drag is just the profile drag of the blade, and is approximated by

$$\begin{aligned} D_{prof} &= \int_{r_R}^{1} dD = \int_{r_R}^{1} \frac{\rho}{2} c\, c_{d_0} V_r^2 R dr\,, \\ &\approx \frac{\rho}{2} c\, c_{d_0} R^3 \Big(\int_{r_R}^{1} \Omega_{mr}^2 r^2 dr - \\ &\quad \int_{r_R}^{1} 2\Omega_{mr}\dot{\xi} r^2 dr\Big)\,, \\ &\approx \frac{\rho}{6} c\, c_{d_0} \Omega_{mr}^2 R^3 \left(1 - r_R^3\right) - \\ &\quad \frac{\rho}{3} c\, c_{d_0} \Omega_{mr}\dot{\xi} R^3 \left(1 - r_R^3\right)\,; \end{aligned} \tag{90}$$

where r_R is the balde root cut-out ratio, i. e., the drag due to the root portion of the blade and hinge has been neglected.

From Equation (90) the aerodynamic damping with respect to blade and hub angular speeds are

$$\left(\frac{\partial D}{\partial \dot{\xi}}\right)_0 \approx -\frac{\rho}{3} c\, c_{d_0} \Omega_{mr_0} R^3 \left(1 - r_R^3\right)\,, \tag{91}$$

$$\begin{aligned} \left(\frac{\partial D}{\partial \Omega_{mr}}\right)_0 &= -\left(\frac{\partial D}{\partial \dot{\xi}}\right)_0 \\ &\approx \frac{\rho}{3} c\, c_{d_0} \Omega_{mr_0} R^3 \left(1 - r_R^3\right) \end{aligned} \tag{92}$$

A.2 Dynamics with Hub Angular Acceleration

The lag acceleration, $\ddot{\xi}$ in Equation (79), is affected by rotor acceleration, $\dot{\Omega}_{mr}$, or vice versa. Also note that the rotor acceleration is caused by a change in torque in the drive train.

Let the engine torque at the rotor speed (Ω_{mr}) be Q_{e_r}, and let the rotor (load) torque be Q_{mr}. A change in Q_{e_r} (or Q_{mr}) results in an angular acceleration (or deceleration) of the rotor hub :

$$J_h\,\dot{\Omega}_{mr} = Q_{e_r} - Q_{mr}\,, \tag{93}$$

where J_h is the hub inertia.

Linearizing the load torque change about a nominal operating condition yields :

$$\begin{aligned} \delta Q_{mr} &\approx eRq_1\Omega_{mr_0}^2 \underbrace{(\xi - \xi_0)}_{\delta\xi} + \\ &\quad eR\left[q_2' + q_3\left(\frac{\partial D}{\partial \dot{\xi}}\right)_0\right]\dot{\xi} \\ &\quad + eR\left[2q_1\Omega_{mr_0}\,\xi_0 + q_3\left(\frac{\partial D}{\partial \Omega_{mr}}\right)_0\right]\delta\Omega_{mr} \\ &\quad + eRq_4\,\dot{\Omega}_{mr}\,, \end{aligned} \tag{94}$$

where Ω_{mr_0} is the nominal value of rotor speed (27 rad/sec), and

$$q_2' \equiv q_2 + q_5\,\Omega_{mr_0}\,\xi_0\,, \tag{95}$$

$$\xi_0 \approx \frac{D_0}{meR\Omega_{mr_0}^2}\,. \tag{96}$$

The angular acceleration can be computed using Equations (93) and (94) :

$$\begin{aligned} \dot{\Omega}_{mr} &= \frac{1}{J_h + eRq_4}(\delta Q_{e_r} - h_\omega\,\delta\Omega_{mr} - \\ &\quad eRq_1\Omega_{mr_0}^2\,\delta\xi - eRq_2''\,\dot{\xi})\,, \end{aligned} \tag{97}$$

where

$$\begin{aligned} h_\omega &\equiv \left(\frac{\partial Q_{mr}}{\partial \Omega_{mr}}\right)_0 \\ &= eR\left[2q_1\Omega_{mr_0}\xi_0 + q_3\left(\frac{\partial D}{\partial \Omega_{mr}}\right)_0\right], \end{aligned} \tag{98}$$

$$q_2'' \equiv q_2' + \underbrace{q_3\left(\frac{\partial D}{\partial \dot{\xi}}\right)_0}_{<0}\,. \tag{99}$$

Similarly, linearizing the lead-lag equation, (79), gives

$$\begin{aligned} \ddot{\xi} &\approx -\frac{mey_g R^2\Omega_{mr_0}^2}{I_{z_Q}}\,\delta\xi - \left[\frac{b_{lh}}{I_{z_Q}} - \frac{y_g R}{I_{z_Q}}\left(\frac{\partial D}{\partial \dot{\xi}}\right)_0\right]\dot{\xi} \\ &\quad + \underbrace{\left[\frac{y_g R}{I_{z_Q}}\left(\frac{\partial D}{\partial \Omega_{mr}}\right)_0 - \frac{2mey_g R^2\Omega_{mr_0}\,\xi_0}{I_{z_Q}}\right]}_{\approx 0}\delta\Omega_{mr} \\ &\quad + \left(1 + \frac{mey_g R^2}{I_{z_Q}}\right)\dot{\Omega}_{mr}\,. \end{aligned} \tag{100}$$

Finally the lead-lag angular acceleration is obtained from Equation (100) and Equation (97) as

$$\begin{aligned}\ddot{\xi} &= -\left(\frac{mey_gR^2}{I_{z_Q}} + c_1 d_1 eRq_1\right)\Omega_{mr_0}^2\,\delta\xi \\ &\quad -\left(\frac{b'_{lh}}{I_{z_Q}} + c_1 d_1 eRq_2''\right)\dot{\xi} \\ &\quad -c_1 d_1 h_\omega\,\delta\Omega_{mr} + c_1\,d_1\,\delta Q_{e_r}\,, \end{aligned} \tag{101}$$

where

$$c_1 \equiv 1 + \frac{mey_gR^2}{I_{z_Q}}\,, \tag{102}$$

$$d_1 \equiv \frac{1}{J_h + eRq_4}\,, \tag{103}$$

$$b'_{lh} \equiv b_{lh} - y_g R\left(\frac{\partial D}{\partial \dot{\xi}}\right)_0\,; \tag{104}$$

and Equations (97) and (101) describe the coupled hub-blade torsional dynamics for a single-bladed, articulated rotor.

References

[1] **[AZA85]** Achgill, D. M. and Zagranski, R. D., "Adaptive Fuel Control Testing." Paper presented at the 41st Annual Forum and Technology Display of the AHS, Ft. Worth, Tx., 1985.

[2] **[BOW78]** Bowes, M. A., "Engine/Airframe/Drive Train Dynamic Interface Documentation." USARTL-TR-78-14, June, 1978. (Kaman Aerospace Investigation Report)

[3] **[BRM76]** Bramwell, A. R. S., *Helicopter Dynamics.* John Wiley & Sons, New York, 1976.

[4] **[CHE80]** Chen, R. T. N., "Effects of Primary Rotor Parameters on Flapping Dynamics." NASA-TP-1431, January, 1980.

[5] **[FRS72]** Fredrickson, C., Rumford, K., and Stephenson, C., "Factors Affecting Fuel Control Stability of a Turbine Engine/Helicopter Rotor Drive System." Journal of AHS, Vol. 17, No. 1, 1972

[6] **[HBE78]** Hanson, H. W., Balke, R. W., Edwards, B. D., Riley, W. W., and Downs, B. D., "Engine/Airframe/Drive Train Dynamic Interface Documentation." USARTL-TR-78-15, October, 1978. (Bell Helicopter Investigation Report)

[7] **[HOY72]** Hohenemser, K. H. and Yin, S. K., "Some Applications of the Method of Multiblade Coordinates." Journal of AHS, July, 1972.

[8] **[JAW90]** Jaw, L. C., *Control of a Helicopter Engine in Low Altitude Flight.* Ph. D. Dissertation, Stanford University, 1990.

[9] **[JON80]** Johnson, W., *Helicopter Theory.* Princeton University Press, 1980.

[10] **[KCT79]** Kuczynski, W. A., Cooper, D. E., Twomey, W. J., and Howlett, J. J., "The Influence of Engine/Fuel Control Design on Helicopter Dynamics and Handling Qualities." Paper presented at the 35th Annual Forum of the AHS, Washington, D. C., 1979.

[11] **[NEB78]** Needham, J. F. and Banerjee, D., "Engine/Airframe/Drive Train Dynamic Interface Documentation." USARTL-TR-78-12, May, 1978. (Hughes Helicopter Division Investigation Report)

[12] **[RIA78]** Richardson, D. A. and Alwang, J. R., "Engine/Airframe/Drive Train Dynamic Interface Documentation." USARTL-TR-78-11, April, 1978. (Boeing - Vertol Division Investigation Report)

[13] **[SAE62]** Society of Automotive Engineers, "Helicopter Engine-Rotor System Compatibility." Aerospace Recommended Practice (ARP) 704, June, 1962.

[14] **[STE79]** Stepniewski, W. Z., *Rotory Wing Aerodynamics* (Volume 1 - Basic Theory of Rotor Aerodynamics). NASA CR-3082, January, 1979.

[15] **[THA78]** Twomey, W. J. and Ham, E. H., "Review of Engine/Airframe/ Drive Train Dynamic Interface Development Problems." USARTL-TR-78-13, June, 1978. (United Technologies - Sikorsky Aircraft Investigation Report)

MODELING ROTOR DYNAMICS WITH ROTOR SPEED DEGREE OF FREEDOM FOR DRIVE TRAIN TORSIONAL STABILITY ANALYSIS

Errata (for Paper III.9.1)

1. Page 1 : September 20, 1990
2. Page 1 : **Subscripts**
3. Page 3 : coordinates of the imaginary axis should be $\sqrt{a^2 b_l^2 - 4ak_l}/2$ and $\sqrt{b_l^2 - 4I_{z_Q} k_l}/2I_{z_Q}$.
4. Page 4 : Equation (10)

$$\begin{bmatrix} \dot{\xi} \\ \ddot{\xi} \\ \dot{\Omega}_{mr} \end{bmatrix} \approx \begin{bmatrix} 0 & 1 & 0 \\ -\left(\frac{k_l}{I_{z_Q}} + \frac{k_l}{J_h}\right) & -\left(\frac{b_l}{I_{z_Q}} + \frac{b_l}{J_h}\right) & \frac{k_l}{J_h} \\ -\frac{k_l}{J_h} & -\frac{b_l}{J_h} & -\frac{b_h}{J_h} \end{bmatrix} \begin{bmatrix} \xi \\ \dot{\xi} \\ \Omega_{mr} \end{bmatrix} + \begin{bmatrix} 0 \\ 0 \\ \frac{Q_{er}}{J_h} \end{bmatrix},$$

5. Page 4 : Equation (11)

$$\begin{bmatrix} \dot{\psi}_b \\ \dot{\Omega}_b \\ \dot{\psi}_{mr} \\ \dot{\Omega}_{mr} \end{bmatrix} \approx \begin{bmatrix} 0 & 1 & 0 & 0 \\ -\frac{k_l}{I_{z_Q}} & -\frac{b_l}{I_{z_Q}} & \frac{k_l}{I_{z_Q}} & \frac{b_l}{I_{z_Q}} \\ 0 & 0 & 0 & 1 \\ \frac{k_l}{J_h} & \frac{b_l}{J_h} & -\frac{k_l}{J_h} & -\left(\frac{b_l}{J_h} + \boxed{\frac{b_h}{J_h}}\right) \end{bmatrix} \begin{bmatrix} \psi_b \\ \Omega_b \\ \psi_{mr} \\ \Omega_{mr} \end{bmatrix} + \begin{bmatrix} 0 \\ 0 \\ 0 \\ \frac{Q_{er}}{J_h} \end{bmatrix}.$$

6. Page 5 : fifth line underneath Equation (23) $2I_{z_Q}\,\Omega_{mr_0}\dot{\beta}_{i_0}\,\delta\beta_i$ (in Equation (23)).
7. Page 9 : Equation (76)

$$\begin{bmatrix} \dot{\psi}_b \\ \dot{\Omega}_b \\ \dot{\psi}_{mr} \\ \dot{\Omega}_{mr} \end{bmatrix} \approx \begin{bmatrix} 0 & 1 & 0 & 0 \\ -\frac{k_l}{I_{z_Q}} & -\frac{b_l}{I_{z_Q}} & \frac{k_l}{I_{z_Q}} & \frac{b_l}{I_{z_Q}} \\ 0 & 0 & 0 & 1 \\ \frac{3k_l}{J_h} & \frac{3b_l}{J_h} & -\frac{3k_l}{J_h} & -3\left(\frac{b_l}{J_h} + \frac{b_h}{J_h}\right) \end{bmatrix} \begin{bmatrix} \psi_b \\ \Omega_b \\ \psi_{mr} \\ \Omega_{mr} \end{bmatrix} + \begin{bmatrix} 0 \\ 0 \\ 0 \\ \frac{Q_{er}}{J_h} \end{bmatrix}.$$

8. Page 9 : second line underneath Equation (76), n_b.